Magnetic Design and Measurement of Model Helical Undulators for the International Linear Collider Positron Source

D.J.Scott,* S.Appleton, J.A. Clarke,† O.B. Malyshev,† B.J.A. Shepherd,† and B. Todd
CCLRC Daresbury Laboratory, Daresbury, Warrington, Cheshire WA4 4AD, UK

D.E. Baynham, T. Bradshaw, A. Brummitt, S. Carr, Y. Ivanyushenkov, J. Rochford
CCLRC Rutherford Appleton Laboratory, Chilton, Didcot, Oxfordshire OX11 0QX, UK

I.R. Bailey,† P. Cooke, J.B. Dainton,† and L. Malysheva†
Department of Physics, University of Liverpool, Oxford St., Liverpool, L69 7ZE, UK

D.P. Barber†
DESY-Hamburg, Notkestraße 85, 22607 Hamburg, Germany

G.A. Moortgat-Pick†
Institute of Particle Physics Phenomenology, University of Durham, Durham DH1 3LE, UK, and CERN, CH-1211 Genève 23, Switzerland

(Dated: August 24, 2006)

A comparison of possible undulator designs for the International Linear Collider positron source has resulted in a super-conducting bifilar wire design being selected. After a comprehensive paper study and fabrication of the two pre-eminent designs the super-conducting undulator was chosen instead of the permanent magnet alternative. This was because of its superior performance in terms of magnetic field strength and quality, operational flexibility and cost. The super-conducting undulator design will now be developed into a complete system design for the full 200 m long magnet that is required.

PACS numbers: 07.85.Qe, 85.70.Ay

I. INTRODUCTION

The baseline design for the International Linear Collider (ILC) positron source is based on multi-MeV photons pair producing in a metallic target [1]. The photons are created by the main electron beam passing through a helical undulator. A source of this kind was first described in 1979 [2] and was adopted for the TESLA collider design as an upgrade to polarized positron production [3].

For the ILC design the high energy (∼150 GeV) electron beam from the electron linac passes through a helical undulator generating ∼10 MeV synchrotron radiation at the first harmonic cut-off. (In the TESLA design, for which this work initially started, the undulator was at the 250 GeV point in the linac and was optimized to produce ∼20 MeV photons at the first harmonic cut-off.) If the circularly polarized (CP) radiation from the helical undulator is selected, for example by photon collimation, then this polarization is transferred to the electron-positron pairs and a polarized positron beam can be generated. The higher the CP rate of the photon beam then the higher the polarization of the resultant positron beam. Theoretical studies and computer analyses have shown that a polarised positron beam could greatly enhance the physics reach of the ILC [4].

A schematic of the current ILC layout with main positron source components is shown in FIG. 1. The length of undulator required is 100 m for an unpolarized positron source and 200 m for a polarized positron source. Recently a proof of principal experiment, Experiment-166 [5], demonstrating polarized positron production using this scheme has been completed at the Stanford Lin-

*Electronic address: d.j.scott@dl.ac.uk; Also at Department of Physics, University of Liverpool, Oxford St., Liverpool, L69 7ZE, UK; Also at The Cockcroft Institute, Daresbury Laboratory, Warrington, Cheshire, WA4 4AD, UK
†Also at The Cockcroft Institute, Daresbury Laboratory, Warrington, Cheshire, WA4 4AD, UK

ear Accelerator Center. Initial results indicate polarized positrons have been created and detected [6].

II. UNDULATOR DESIGN

In the ILC baseline design a helical undulator with a period, $\lambda_u = 10$ mm and an undulator K parameter of 1 is assumed. Where K is a dimensionless parameter that is defined as:

$$K = \frac{Be\lambda_u}{m_e c 2\pi},$$

where B is the peak on-axis magnetic field, m_e is the electron mass, e the electron charge and c the speed of light. The maximum angle of deflection experienced by an electron in an undulator is given by the K parameter divided by the the relativistic γ of the electron.

A helical undulator with these parameters has not been experimentally demonstrated yet. A paper study into various helical undulator designs based on permanent magnet (PM) and super-conducting (SC) undulators was carried out. Model test pieces of the most promising designs were constructed to assess the ease of fabrication and to confirm the magnetic field strength and quality.

A. Pure Permanent Magnet Designs

Synchrotron light sources have used planar arrays to produce on-axis helical field distributions for over 20 years. For light sources the planar configuration suits the large horizontal to vertical beam size ratio. Planar helical undulators offer a number of advantages as they are a proven technology with well understood engineering solutions. They also allow easy access to the vacuum vessel which is required if a non-evaporable getter (NEG) coated vessel is used. Three different planar helical PM undulators were considered, the multi-mode undulator [7, 8], the APPLE-II [9], and a new APPLE design, the APPLE-III [10].

A helical field can also be created by using an array of stacked dipole rings in which the dipole field is rotated from ring to ring. Each period of the undulator is divided up into rings. Each ring comprises of trapezoidal PM blocks that produce an on-axis transverse dipole field by rotating the magnetization vector of the PM blocks by 4π radians around the ring [11] (shown in FIG. 2 for 8 magnet blocks in a ring). The dipole field of each ring is rotated with respect to the preceding one so that over one period the total rotation of the on-axis dipole field is 2π radians [12].

The different undulator designs were modeled in the magneto-statics code Radia [13] to find the peak on-axis magnetic field, B. The planar undulators were modeled in circularly polarizing mode. Figure 3 shows λ_u vs B for each model as well as the required period and field to produce 20 MeV photons with a 250 GeV beam and 10 MeV photons with a 150 GeV beam. The PM material used was NdFeB with a remenant magnetization of 1.3 T. As expected the PM ring undulator out-performs the planar helical undulators as there is magnetic material surrounding the vacuum chamber driving more flux into the aperture.

The multi-mode undulator has 6 arrays compared to the APPLE-II and APPLE-III's four arrays which means it can produce a high on-axis field in circularly polarizing mode. The APPLE-III design has notches cut into the magnet blocks so they are closer to the magnetic axis giving a higher field on-axis than the APPLE-II design. To minimize the total length of undulator required the 14 mm period PM ring undulator was chosen. (N.b. some of the parameter choices made in this study reflect the fact that this work was initially started for the TESLA project, and may not be fully-optimised for the ILC baseline.)

To achieve the preferred vacuum in the vessel of 10^{-8} mbar (CO equivalent) the vacuum vessel would need to be coated with a NEG coating. NEG coating requires activation by bakeout and so access to the vessel would be required. Therefore the undulator was designed to be split into two halves, since the baking required to activate the NEG would otherwise demagnetize the PM blocks. To keep the design regular (i.e. smooth along the faces of each half) the number of blocks per ring must be an even number and must be a multiple of the number of rings per period.

Another issue that was considered is the magnetic force between the arrays. The force between the two undulator halves can be considerable and depends on the detailed configuration of the magnet blocks. Figure 4 shows the magnet forces between the arrays for ten periods of a 14 mm period device as a function of the array gap. The first number in the legend refers to the number of PM blocks making a ring and the second number gives the number of rings in a period. It can be seen that the force between the two halves can either be repulsive or attractive, depending upon the configuration. A typical length for a PM undulator would be 5 m and so the forces between the arrays could be as high as 30 kN at zero magnetic gap. This would make the engineering of the support girders and gap control mechanism quite demanding. To make the supporting structure as simple as possible an 8 blocks per ring/8 rings per period configuration was chosen as this minimizes the forces between each array at all gaps.

A ten period model was chosen to be made to allow for measurement of the magnetic field away from any end effects. Wedges of PM material were made up of identically shaped pieces with a rotated axis of magnetization (left side of FIG. 5). Four wedges were then glued into aluminium holders to make half of a ring (center of FIG. 5). The aluminium holders were then aligned and fastened to top and bottom array base plates, which could then be fitted together in the final assembly (right

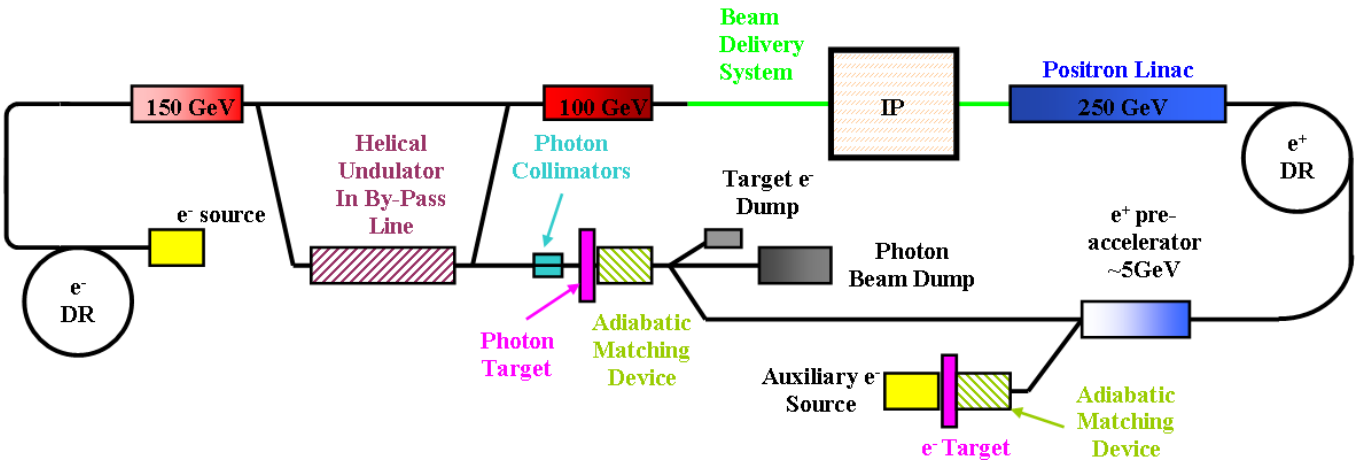

FIG. 1: (Color) ILC schematic layout with main positron source components. The undulator is placed at the 150 GeV point of the main linac in a by-pass line so that the axis of the generated photon beam is separate from the axis of the main electron beam. Photons incident on the target produce electron-positron pairs via pair production. The positrons are captured and accelerated in the adiabatic matching device and then accelerated to 5 GeV in the pre-accelerator. They are then transported to the positron damping ring and then on to the main positron linac. DR stands for the damping rings and the auxiliary electron source represents a low intensity conventional positron source to be used when the undulator source is not functioning.

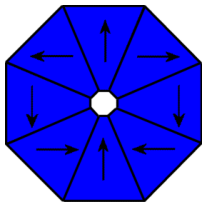

FIG. 2: (Color) Schematic showing the magnetization vectors of a dipole ring comprising of 8 magnet blocks. For 8 blocks in a ring the magnetization vector must be rotated by 90° from block to block to produce a dipole field on-axis.

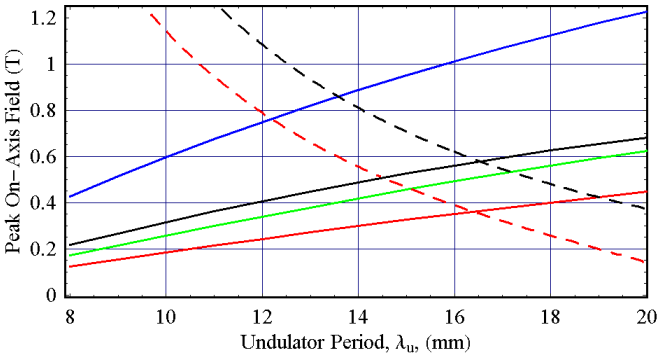

FIG. 3: (Color) Computer modeled peak on-axis magnetic field for APPLE-II (solid, red), APPLE-III (green), multi-mode (solid, black) undulators in circular polarizing mode and for the PM ring undulator (blue) vs undulator period length. The field/period length required to produce 10 MeV photons with 150 GeV electron beam (dashed, red) and 20 MeV photons with a 250 GeV beam (dashed, black) at the first harmonic is also shown.

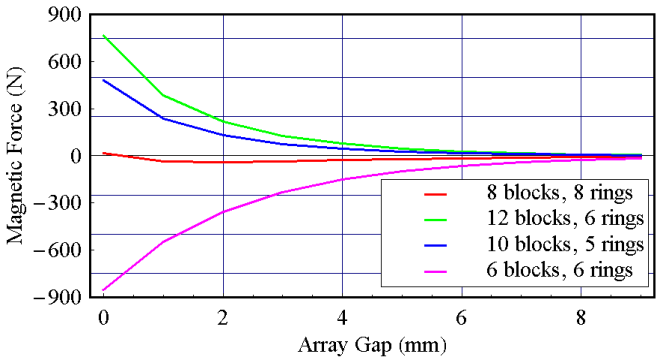

FIG. 4: (Color) Magnetic forces between the arrays for 10 periods of different PM ring undulator configurations. The legend gives the number of blocks making a single ring and the number of rings making a period.

side of FIG. 5). A photograph of the completed undulator is shown in FIG. 6.

B. Super-Conducting Magnet Design

This design is based on two helical super-conducting windings wound around a vacuum vessel. The windings are spatially shifted a half period in the longitudinal direction and current is passed through each winding in opposite directions. With current flowing the on-axis longitudinal magnetic field cancels leaving only a helical transverse field. A number of devices have been made in this manner, [14, 15].

Extensive magnetic modeling was carried out in order to select the winding geometry of the undulator [16]. The software packages OPERA 2d and 3d from Vector Fields

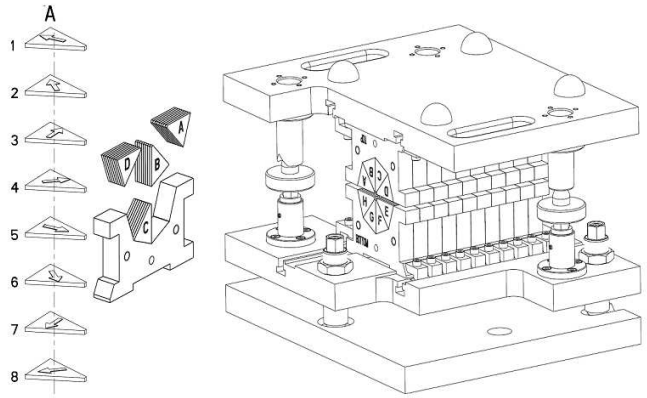

FIG. 5: Assembly drawing of PM ring undulator.

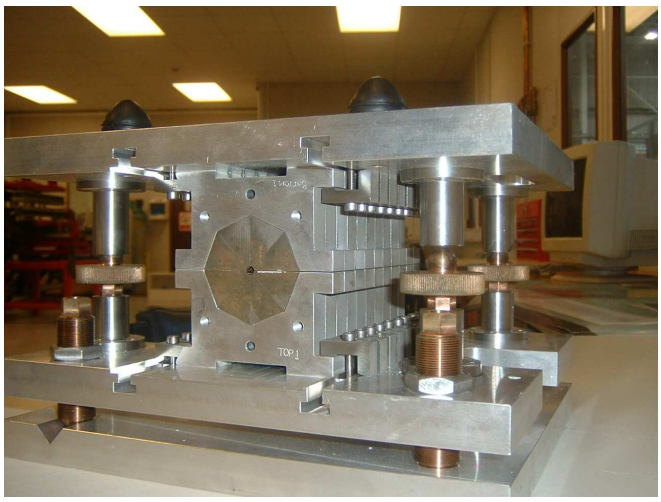

FIG. 6: (Color) Photograph of completed PM ring undulator assembly, with ten 14 mm periods.

Ltd [17] were used for the modeling studies. The results of the magnetic modeling indicate that:

- A winding with a flat shape (with the minimal radial height to width ratio) creates maximal field on-axis for a given current density. However, taking into consideration the peak field in the conductor, a square shape was found to be optimal.
- The peak field in the conductor is about twice the field on the undulator axis. The highest field in the conductor is always in the internal layers of the winding (FIG. 7).

Undulator conductor load lines, shown in FIG. 8, were calculated for a winding geometry of 8 layers with 8 wires in a layer and for 8 layers with 9 wires in a layer. The 9x8 winding operates at 86% of the critical conductor giving a safety margin of 14%. The 8x8 winding operates at 94% of the critical current and the safety margin is 6%. The prototype uses an 8×8 winding geometry as it was not possible to fit a 9-wire ribbon into the rectangular groove

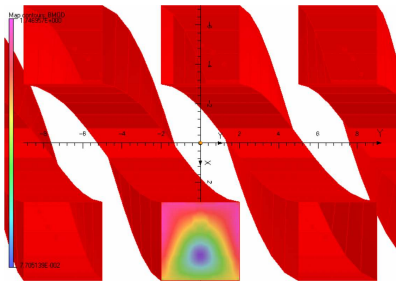

FIG. 7: (Color) Calculated magnetic flux density through a cross-section of the conductor windings for a current density of 1000 $A\ mm^{-2}$. The highest flux is in pink near the axis of the magnet and is 1.75 T. The lowest flux is in blue near the centre of the winding and is 77 mT.

of the first former. Future former designs will be made trapezoidal to accommodate a 9-wire ribbon. A period of 14 mm was chosen as the computer model predicted the required field could be achieved. This also allowed for a fair comparison with the PM magnet.

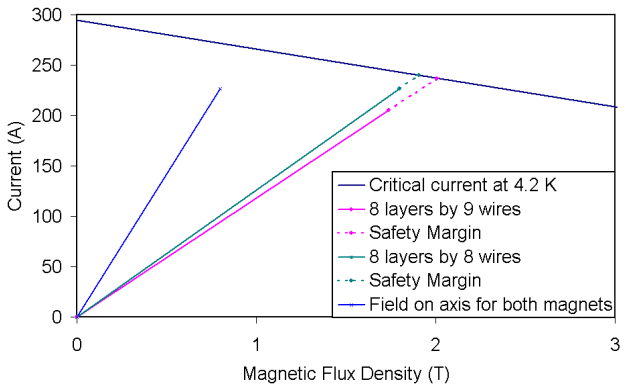

FIG. 8: (Color) Undulator conductor load lines, critical current at 4.2 K and the field achieved on-axis.

FIG. 9: (Color) Photograph of undulator winding showing the return pegs to allow for continuous winding.

The undulator was wound with super-conducting wire, VACRYFLUX 5001 type F54 [18], onto an aluminium former 20 periods long. Preliminary work on the winding indicated that winding the undulator with a wire ribbon

could significantly reduce technical difficulties encountered at the ends of the multi-wire winding. A similar approach is implemented at CERN for the winding of Large Hadron Collider corrector magnets [19].

Eight 0.44 mm wires were bonded in a flat ribbon with a width of approximately 4 mm and a thickness of 0.5 mm. The ribbon was then wound into a spiral groove in the former. To achieve a continuous winding of two helices in one operation, two sets of pegs were used at the ends of the undulator for the return of the ribbon into the adjacent helical groove (FIG. 9).

After winding, the undulator coil was vacuum impregnated with epoxy resin and the wires in the ribbon were interconnected at the terminal block to form the series winding. As a result, the undulator winding forms a multi-layer, continuous, double-helical, winding with two leads for connection to a power supply. The final view of the undulator before installation into the cold test rig is shown in FIG. 10.

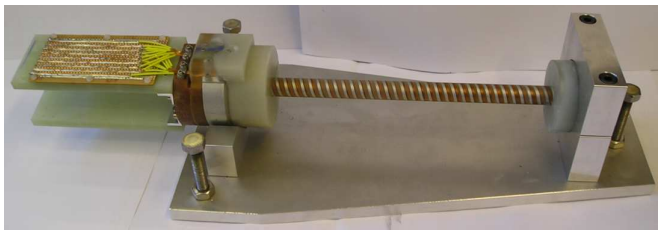

FIG. 10: (Color) Photograph of the completed SC undulator before field measurement, with twenty 14 mm periods.

III. MAGNETIC MEASUREMENTS

After fabrication of the two models magnetic field measurements were taken and these are detailed below.

A. PM Ring Undulator Measurements

The direction and magnitude of the magnetization vector for each individual magnet block was measured before assembly and their position in the assembly recorded. From this data the expected magnetic field was calculated in Radia. The on-axis field of the assembled magnet was measured using a conventional hall probe measuring bench. The probe was mounted on a stiff carbon fibre shaft and aligned to the axis of the bench. Figure 11 shows the measured field, expected measurements (from the individual block data) and ideal field in the two transverse directions, x and y, respectively. First and second field integrals in the transverse directions ($I_{x,y}$, $J_{x,y}$), undulator K parameters and the mean on-axis peak field neglecting the ends are given in Table I. For a 150 GeV electron beam the final angle at the end of the undulator is 6.4 and 2.9 μrad in the x and y direction respectively. The final displacement off axis is 0.65 and 0.26 μm in the x and y directions respectively.

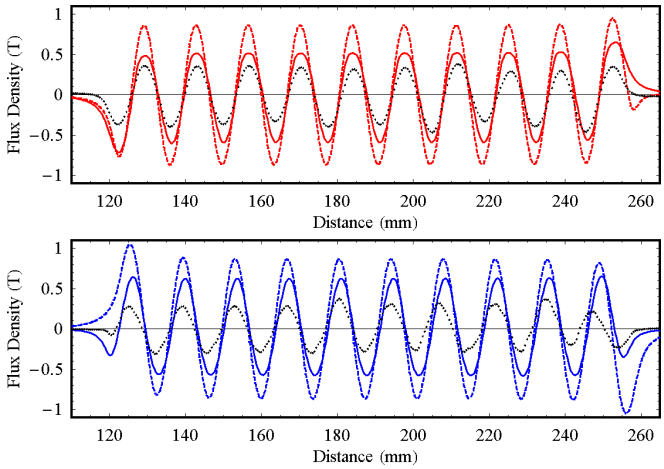

FIG. 11: (Color) Ideal (dashed), computer model based on actual block measurements (solid) and measured (points) on-axis magnetic flux density in the x direction (top) and y direction (bottom) for the PM ring undulator.

The computer modeled field is less than the ideal field due to the magnetization errors of the individual magnet blocks. As the ILC polarized positron source requires an undulator 200 m in length, it is important to minimize the costs of individual magnets where possible. Relaxed specifications requiring lower production costs were therefore chosen for the permanent magnets in order to ascertain whether the required field could be realised economically. The tolerance on the deviation of the magnetisation vector direction from the ideal direction was specified to be $\pm 3^\circ$, after thermal stabilisation, compared to $\pm 1.5^\circ$ commonly used in undulators for synchrotron light sources. Therefore the modeling indicates that high quality magnet blocks should be used if the ideal peak field is to be obtained.

The measured field is less than was expected from the computer model, this could be due to a number of effects. Although every effort was made to ensure each block was measured accurately and aligned correctly in the assembly mistakes may have been made. Also, the strong demagnetizing field that blocks experience when bonding the wedges, bonding the wedges into the holders and then bringing the two arrays together could have reduced their remanant field strength and working point. As can be seen from the comparison of the ideal and computer modeled results, the magnetization vector errors can result in a decrease in the peak field strength of $\sim$0.15 T. It is also possible that the coercivities of the magnet blocks were less than the design specification of 950 kA m^{-1}, making them easier to de-magnetize. To accurately test these hypotheses would require the magnet to be disassembled and the magnetic field strength and direction of the individual blocks re-measured. However this is impractical due to the strength of the bonding

TABLE I: PM and SC undulator field measurement data.

Parameter	Unit	PM Und.	SC Und.
I_x, I_y	T mm	-3.2, 1.5	1.4, 1.8
J_x, J_y	T mm^2	-0.064, 0.056	0.27, 0.046
K_x, K_y		0.52, 0.45	0.99, 0.98
On-Axis Peak Field	T	0.30, 0.36	0.81, 0.81

and the low intrinsic strength of the individual magnet blocks.

B. SC Undulator Measurements

The undulator was mounted vertically in a liquid helium bath. The level of liquid helium in the cryostat was monitored with discrete level sensors to ensure that liquid helium covered both the undulator coil and the super-conducting current leads. The temperature of the undulator was monitored during cool-down and operation. Voltage taps were used to measure the resistive voltage across the undulator coil with a nano-voltmeter when the undulator was powered. In the cold test the undulator reached the maximum current of the power supply at 225 A without quenching. The voltage across the complete undulator coil was at the level of 10^{-6} V. This indicates that the wire interconnections have a total resistance $< 10^{-8}$ Ω. The undulator field profile, measured at a current of 220 A, is shown in FIG. 12 and has the expected peak field. The first and second field integrals, K parameters and mean on-axis peak field data are given in Table I. For a 150 GeV electron beam the final angle at the end of the undulator is 2.9 and 3.6 μrad in the x and y direction respectively. The final displacement off axis is 0.45 and 0.53 μm in the x and y directions respectively.

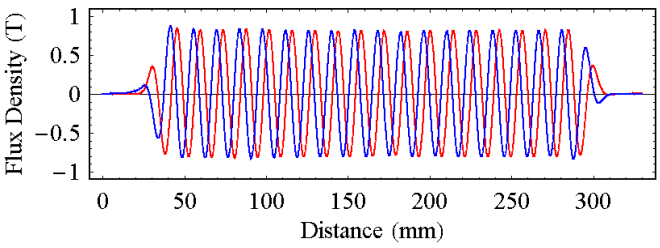

FIG. 12: (Color) Measured on-axis magnetic field in both transverse directions for the SC undulator.

IV. PHOTON FLUX AND POLARIZATION

From the measured magnetic field of the undulators the radiation spectrum and polarization can be calculated. This was done using the numeric code SPECTRA [20] and is shown in FIG. 13 for an ILC beam with

TABLE II: ILC beam parameters used for flux and polarization calculation.

Parameter	Unit	Value
Beam Energy	GeV	150, 250
Average Current	μA	45
Natural Emittance	nm rad	2 10^{-2}
Average β	m	25
Relative Energy Spread		0.0006

parameters as given in Table II for the two different models. Two different beam energies have been considered to show the difference between the TESLA and ILC designs. Table III gives the peak flux and circular polarization rate.

Due to interference effects, characteristic of all undulator radiation, there will be some spectral broadening in the photon spectrum due to the finite length of the undulators. The FWHM of the ten period PM undulator device is approximately a factor of two larger than the FWHM of the twenty period superconducting device for each harmonic peak, as can be seen in the widths of the first harmonics in FIG. 13. For the real ILC undulator this would not be a significant factor as both devices would have many thousands of periods. The difference between the total number of photons for the two undulators is explained by the differing K parameters. The total photon flux scales linearly with the undulator length and determines the maximum positron intensity in the ILC positron source. As the PM undulator produces less photons per unit length it would consequently have to be longer to produce the same positron intensity as the the SC undulator. The circular polarization rates are between 0.78 and 0.93 and although there is no specification for the ILC it is assumed that these rates, being close to the ideal value of 1, are acceptable. The polarisation rates for the SC undulator results are higher than those for the PM undulator because the magnetic field quality in the SC undulator is better.

V. CONCLUSIONS AND FURTHER WORK

An investigation into possible helical undulator designs for the ILC positron source has been carried out. Based on the paper design work two model undulators were constructed to assess the ease of fabrication and magnetic field quality. Both undulators produced a helical field distribution. The SC undulator performed to expectations but the PM one did not. For the PM ring undulator the field quality and strength were both less than expected.

This was probably due to the large number of components leading to possible assembly errors and possible de-magnetization of the individual PM blocks. A tighter specification of magnet block errors would have ameliorated some of these problems, whilst the de-

TABLE III: Peak flux and circular polarization values for SC and PM undulaotrs.

Parameter	Unit	PM (150 GeV)	PM (250 GeV)	SC (150 GeV)	SC (250 GeV)
Peak Flux Energy	MeV	12.1	33.4	6.8	19.0
Peak Flux	10^{10} Ph./period s^{-1} 0.1%	2.1	2.4	7.8	9.1
Peak CP Energy	MeV	12.0	33.4	6.8	19.1
Peak CP rate		0.84	0.78	0.92	0.83

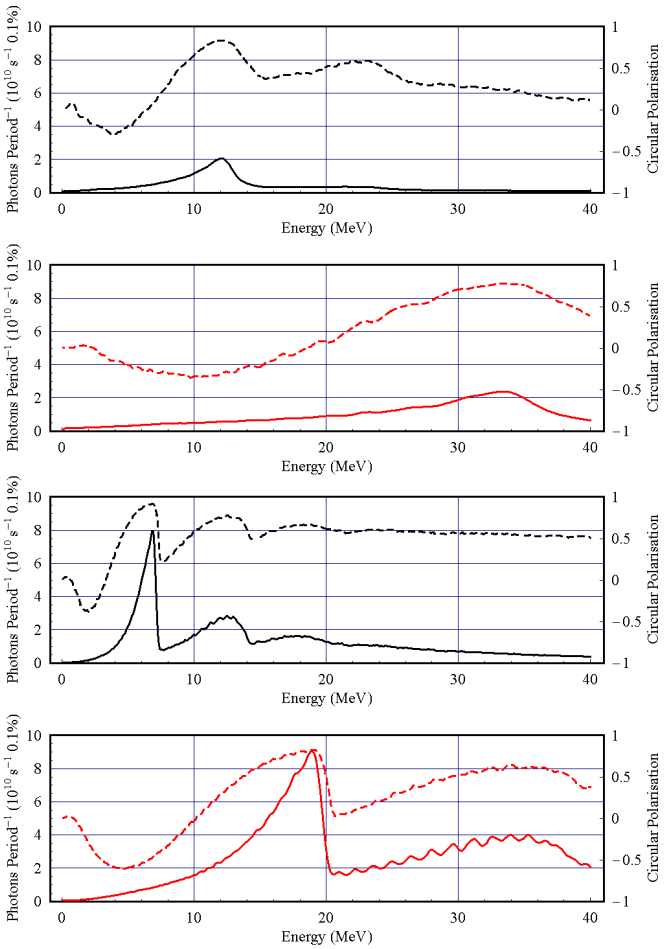

FIG. 13: (Color) Photon spectrum per period (solid) and circular polarization rate (dashed) from PM ring undulator (top) and SC undulator (bottom) for 150 GeV (black) and 250 GeV (red) energy electrons. Calculated using the measured magnetic flux density data.

magnetization effects would have been reduced if blocks with a higher coercivity had been manufactured. However, this would have increased the production costs significantly.

In terms of operational aspects the SC undulator is favored as the on-axis magnetic field can be controlled easily, allowing for a variable undulator K parameter. The SC undulator is also easy to switch off, whereas the PM ring magnet would have to have a gap control mechanism and support for the vacuum chamber in order to reduce the field on-axis to negligible levels. This is achievable but more involved than for the SC undulator. For the vacuum requirements the PM ring undulator would need significant development of a NEG coated vessel due to the small aperture of the magnet (the SC undulator relies on cryo-pumping to achieve a vacuum). It is also unclear at the present time what the impedance effects of the NEG coating on the electron beam would be.

For these reasons the super-conducting undulator has now been selected for the ILC positron source.

Further work will look at the design of a SC undulator in more detail. The inclusion of iron poles and an iron sleeve will be considered to increase the on-axis flux. A re-optimisation of the parameters, to account for the undulator being at the 150 GeV part of the linac, will also be completed. A full scale working prototype with cryostat will then be fabricated and tested with an electron beam.

Acknowledgments

The authors gratefully thank members of the Magnets and Electrical Systems Group of the CERN Accelerator Technology Department for their help in the manufacture of the super-conducting wire ribbon. The work is also supported by the Commission of the European Communities under the 6th Framework Programme Structuring the European Research Area, contract number RIDS-011899.

[1] ILC Baseline Configuration Document (BCD), http://www.linearcollider.org/wiki/.
[2] V. E. Balakin and A. A. Mikhailichenko, BINP 79-84 (1977).
[3] *TESLA Technical Design report*, DESY, (2001).
[4] G. A. Moortgat-Pick et al. (POWER Collaboration), arXiv:hep-ph/0507011, (Submitted to Physics Reports).
[5] G. Alexander et al. (E166 Collaboration), SLAC-PROPOSAL-E166, (2001).
[6] K. T. Macdonald et al. (E166 Collaboration), in *Proceedings of the 10th European Particle Accelerator Conference*, Edinburgh, 2006.

[7] A. Hiraya, K. Yoshida, S. Yagi, M. Taniguchi, S.-Kimura, H. Hama, T. Takayama and D. Amano, J. Synchrotron Rad. **5**, 445 (1998).
[8] G. V. Rybalchenko, K. Shirasawa, M. Morita, N. V. Smolyakov, K. Goto, T. Matsui and A. Hiraya, Nucl. Instrum. Methods A **467-468**, 173 (2001).
[9] S. Sasaki, K. Miyata1 and T. Takada, Jpn. J. Appl. Phys. **31**, L1794 (1992).
[10] *The BESSY Soft X-ray Free Electron Laser Technical Design Report*, BESSY, (2005).
[11] K. Halbach, Nucl. Instrum. Methods **169**, 1 (1980).
[12] M. S. Curtin, S. B. Segall and P. Diament, Nucl. Instrum. Methods A **237**, 395 (1985).
[13] P. Elleaume, O. Chubar and J. Chavanne, in *Proceedings of the 6th European Particle Accelerator Conference*, Stockholm, 3509, (1998).
[14] L. R. Elias and J. M. J. Madey, Rev. Sc. Instrum. **50** 1335 (1979)
[15] T. A. Vsevolozhskaya, A. D. Chernyakin, A. A. Mikhailichenko, E. A. Perevedentsev and G. I. Silvestrovk, in *Proceedings of the XIII International Conference in High Energy Accelerators*, Novosibirsk, (1986).
[16] J. Rochford et al. (Helical Collaboration), in *Proceedings of the 10th European Particle Accelerator Conference*, Edinburgh, 2006.
[17] Vector Fields Ltd, 24 Bankside, Kidlington, Oxford OX5 1JE, UK
[18] VACUUMSCHMELZE GmbH, D 63412 Hanau, Germany.
[19] D. Bayham, R. Coombs, A. Ijspeert and R. Perin, IEEE Trans. Magn. **30**, 1823, No 4, (1994).
[20] T. Tanaka and H. Kitamura, J. Synchrotron Rad. **8**, 1221 (2001).